

Self-organization of local streamline structures and energy transfer rate in compressible plasma turbulence

SIMONE BENELLA ,¹ VIRGILIO QUATTROCIOCCHI ,¹ EMANUELE PAPINI ,¹ ANDREA VERDINI ,² SIMONE LANDI ,²
 MARIA FEDERICA MARCUCCI ,¹ AND GIUSEPPE CONSOLINI ,¹

¹ INAF - Institute for Space Astrophysics and Planetology, Via del Fosso del Cavaliere, 100, 00133, Rome, Italy

² Dipartimento di Fisica e Astronomia, Università di Firenze, Via G. Sansone 1, Sesto Fiorentino (Firenze), 50019, Italy

ABSTRACT

We examine how local streamline topology and energy cascade rate self-organize in plasma turbulence for both compressible and incompressible regimes. Using a fully-compressible Hall-magnetohydrodynamic simulation, we quantify the subgrid-scale energy transfer and analyze its relationship to streamline structures by means of gradient tensor geometric invariants of the velocity field. Our results highlight how streamline topology is crucial for diagnosing turbulence: for nearly-incompressible fluctuations the energy is primarily transferred to smaller scales through strain-dominated and stable-vortical structures, while is back-transferred towards larger scales through unstable-vortical structures. Compressible fluctuations, on the contrary, do not show a clear topological selection of the energy transfer since the overall direction of the local cascade rate is found to be determined by the sign of $-\nabla \cdot \mathbf{u}$ (plasma volumetric compression or expansion).

Keywords: Space plasmas (1544) — Interplanetary turbulence (830) — Heliosphere (739) — Solar wind (1534)

1. INTRODUCTION

Turbulence in space plasmas remains a major open problem, despite significant advances from theory, improved spacecraft in situ measurements, and numerical simulations (R. Bruno & V. Carbone 2016). In a turbulent plasma, the large-scale energy budget is transferred across the magnetohydrodynamic (MHD) inertial range toward ion scales through a cascading process that generates a hierarchy of structures at all scales. Observational and numerical studies have shown that while the average direction of the energy transfer is predominantly forward, inverse energy transfer can also occur at all scales. In the case of incompressible plasmas, for example, the emergence of inverse cascade has been linked to the imbalance between counter propagating Alfvén waves, suggesting a dependence of the local energy transfer to the large-scale organization of the turbulent fluctuations (C. W. Smith et al. 2009; J. E. Stawarz et al. 2010; J. T. Coburn et al. 2014). In addition to the local energy transfer associated with nonlinear interactions, at ion scales kinetic instabilities and other nonlocal processes can significantly contribute to the energy

transfer. For instance, magnetic reconnection occurring at sub-ion scales has been shown to induce an inverse energy transfer toward MHD scales (L. Franci et al. 2017; D. Manzini et al. 2023; R. Foldes et al. 2024). An heuristic proxy of the energy transfer rate, which is local in time (space), hence called *local energy transfer* (LET), has been introduced by L. Sorriso-Valvo et al. (2018) in the context of numerical simulations. This quantity provides useful insights about the irregular and burst-like activity associated with the transfer rate from and towards small scales, and possibly constituting an indirect proxy of turbulent structures. The operative definition of the LET is based on the Yaglom's law (H. Politano & A. Pouquet 1998; R. Marino & L. Sorriso-Valvo 2023), which is averaged on a fixed short time window, allowing to assess the locality of the energy transfer in time. The deep link between LET and kinetic plasma properties has been emphasized by (L. Sorriso-Valvo et al. 2019), where the LET has been estimated on Magnetospheric Multiscale (MMS; J. L. Burch et al. 2016) measurements.

As energy flows across scales, turbulence organizes in a hierarchy of coherent, multiscale structures. An effective way of investigating the local properties of such behavior is based on the statistics of the gradient-tensor

geometrical invariants (GTGIs). The first investigation of the properties and the lagrangian dynamics of GTGIs has been provided by P. Vieillefosse (1982), who introduced the evolution equation of GTGIs for a restricted Euler system (see also P. Vieillefosse 1984). This simple theoretical framework has been later extended to more sophisticated models, such as shell models by L. Biferale et al. (2007), (see C. Meneveau 2011, for a review). The typical hallmark of energy dissipation in the statistics of the GTGIs consists of an asymmetric feature called the *Vieillefosse tail*. In addition to the lagrangian time evolution of GTGIs, further investigations also elucidated the scale dependent behavior of GTGI statistics. M. Chertkov et al. (1999) showed that by coarse-graining the velocity field, the Vieillefosse tail tends to disappear when moving towards the inertial range. In the framework of MHD simulations, V. Dallas & A. Alexakis (2013) investigated the statistics of GTGIs of velocity and magnetic fields by means of MHD direct numerical simulations providing an extension of earlier hydrodynamic theories.

First observational evidence of the presence of the Vieillefosse tail in the GTGI statistics in space plasmas was reported in G. Consolini et al. (2015) leveraging the multipoint measurements provided by the Cluster spacecraft constellation (C. P. Escoubet et al. 1997). In that work, authors showed that the typical asymmetry in the velocity-field gradients routinely observed in hydrodynamics is also present in the solar wind. Conversely, the absence of this feature in the magnetic field GTGIs, reported by V. Dallas & A. Alexakis (2013) in MHD simulations, has been confirmed by numerous studies based on data gathered by Cluster and Magnetospheric Multiscale (MMS) missions (V. Quattrociocchi et al. 2019; B. Hnat et al. 2021; J. Zhang et al. 2023; V. Quattrociocchi et al. 2025). All these works provide important clues on the properties of turbulent systems by quantifying the statistics of the formation of local structures, but their relation to the energy transfer has not been fully assessed yet. Evidence of the existing correlation between the energy transfer rate and the GTGIs, which elucidates how the local topology of streamline structures connects to the local turbulent cascade, has been introduced in the context of hydrodynamics (F. van der Bos et al. 2002; A. Vela-Martín & J. Jiménez 2021; H. Yao et al. 2024). In the field of space plasmas, the crucial interplay between field line topology and LET has been assessed by B. Hnat et al. (2025) for the magnetic field. They show that positive LET (i.e., direct energy cascade) exhibits a significant correlation with the occurrence of strain-dominated magnetic field structures, suggesting the crucial role of fundamental

processes, such as magnetic reconnection, in driving the energy cascade. Another key aspect of all these studies presenting the statistics of GTGIs in space plasmas is that they rely on the assumption of incompressibility, which is encoded in the GTGI equations used in the data analysis. In this context, the aim of this letter is two-fold: to reveal the intimate relation between local streamline topology and energy transfer rate, and to investigate and compare this connection in both compressible and incompressible cases. All these steps are carried out by analyzing a three-dimensional Hall-MHD numerical simulation of plasma turbulence.

2. THE GEOMETRIC INVARIANTS OF THE GRADIENT TENSORS

The method adopted in this work relies on the geometric invariants of the velocity field gradient tensor $\mathbf{A} = \nabla \mathbf{u}$. To define invariants quantities, we introduce the characteristic polynomial of the gradient tensor. Starting from the expression of this polynomial, it is possible to define characteristic quantities that are invariant under $SO(3)$ -group transformations (i.e., rotations and reflections). These quantities are related to the trace and the determinant of the matrix. The three gradient tensor geometric invariants (GTGIs) thus are

$$P = -\text{Tr}(\mathbf{A}) = -(\lambda_1 + \lambda_2 + \lambda_3) \quad (1)$$

$$Q = \frac{1}{2}(P^2 - \text{Tr}(\mathbf{A}^2)) = \lambda_1\lambda_2 + \lambda_2\lambda_3 + \lambda_3\lambda_1 \quad (2)$$

$$R = -\det(\mathbf{A}) = -\lambda_1\lambda_2\lambda_3, \quad (3)$$

where $\lambda_i, i = 1 \dots 3$ are the eigenvalues of \mathbf{A} , which encode fundamental information on the local flow topology. Denoting by λ_1 the real eigenvalue, the remaining pair λ_2, λ_3 may be either real (pure strain) or complex conjugate (vortical motion). In the latter case, the sign of $\text{Re}\lambda_{i=2,3}$ determines whether the local topology is stable ($\text{Re}\lambda_{i=2,3} < 0$) or unstable ($\text{Re}\lambda_{i=2,3} > 0$). When all the eigenvalues are real, the stability is instead expressed by the sign of $\lambda_2 + \lambda_3$, i.e., the net contraction or expansion on the plane orthogonal to the principal direction. The sign of the principal eigenvalue λ_1 indicates compressing ($\lambda_1 < 0$) or stretching ($\lambda_1 > 0$) topologies. For incompressible flows ($P = 0$), the divergenceless constraint $\lambda_1 = -(\lambda_2 + \lambda_3)$ couples the dynamics along the principal direction to the transverse plane. Consequently, an unstable transverse topology ($\lambda_2 + \lambda_3 > 0$) necessarily implies a compression with rate $-(\lambda_2 + \lambda_3)$ along the principal direction, and vice versa. In other words, flow configurations including simultaneous contraction (“sinks”) or dilation (“sources”) along all the directions are forbidden. In the compressible flows ($P \neq 0$), this constraint is relaxed and

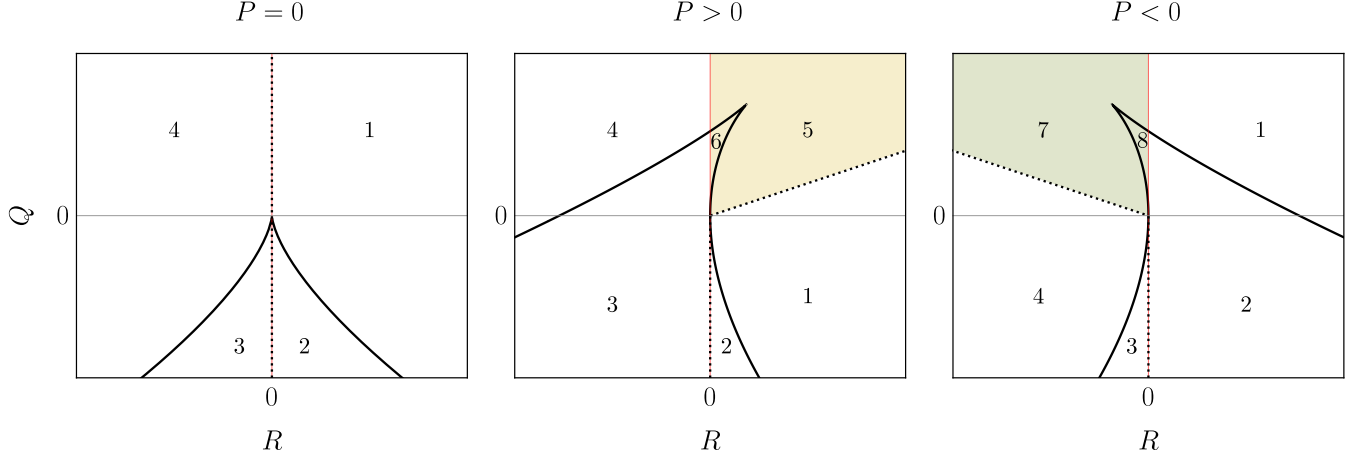


Figure 1. Sketch of the local streamline topologies in the RQ -plane for the three cases $P = 0$ (left), $P > 0$ (middle), and $P < 0$ (right). Thick line is the discriminant surface Δ . Red line marks the separation between stretching and compressing regions, and the dashed line indicate the separation between stable and unstable topologies. Shaded areas indicate topologies associated with local volumetric contraction (yellow) and expansion (green) emerging in compressible cases only.

additional topologies, such as local volumetric expansion or contraction along all directions, become admissible (S. Suman & S. S. Girimaji 2010; L. Wang & X.-Y. Lu 2012; N. S. Vaghefi & C. K. Madnia 2015; Q. Zheng et al. 2022). By considering the case of negative divergence ($P > 0$), we can write the condition $\lambda_1 < -(\lambda_2 + \lambda_3)$, which implies that unstable transverse topologies are always associated with a compression stronger than $-(\lambda_2 + \lambda_3)$ on the principal direction, thus precluding the formation of local sources. Conversely, for the positive divergence case ($P < 0$), simultaneous contractions along all direction is locally forbidden, since the condition $\lambda_1 > \lambda_2 + \lambda_3$ holds in this case. In other words, stable transverse topologies are always coupled with a stretching rate larger than $\lambda_2 + \lambda_3$ along the principal direction λ_1 , effectively preventing the formation of local sinks.

The surface that divides the real solutions from the complex ones is given by the discriminant line

$$\Delta = 27R^2 + (4P^3 - 18PQ)R + (4Q^3 - P^2Q^2) = 0, \quad (4)$$

which in the incompressible case reduces to

$$\Delta|_{P=0} = 4Q^3 + 27R^2 = 0. \quad (5)$$

This surface separates the RQ -plane in two parts (see Figure 1, left panel), the $\Delta|_{P=0} > 0$ region where we find vortical compressing (1) and stretching (4) structures (one real and two complex-conjugate eigenvalues), and the $\Delta|_{P=0} < 0$ region, where the streamline are subject to pure compressing (2) or stretching (3) strain (three real eigenvalues). The compression/stretching separation in the $R = 0$ line, that in the incompressible case coincides with the stable/unstable separatrix $PQ - R = 0$. When $P > 0$, in addition to the topologies from (1)

to (4), the simultaneous modification of the Δ surface along with the stable/unstable separatrix that deviates from the line $R = 0$, induces two new topologies: stable compressing vortical (5) and strain (6) structures, i.e., local sinks (Figure 1 middle panel). Analogous considerations explain the emergence of two opposite topologies in the case $P < 0$ (Figure 1, right panel) which are unstable stretching vortical (7) and strain (8) structures, thus acting as local sources (N. S. Vaghefi & C. K. Madnia 2015).

3. COARSE-GRAINING AND ENERGY TRANSFER RATE

To investigate the local energy cascade rate across a scale ℓ , we introduce a coarse-graining (CG) based on the space-filter approach (M. Germano 1992; G. L. Eyink 2005; H. Aluie & G. L. Eyink 2010; H. Aluie 2017; E. Camporeale et al. 2018; D. Manzini et al. 2022; R. Foldes et al. 2024), where the CG consists of a Gaussian kernel $G_\ell(\mathbf{x}) = \ell^{-3}G(\mathbf{x}/\ell)$ with zero mean and unit variance, i.e.,

$$\bar{f}(\mathbf{x}) = \int d\mathbf{r} G_\ell(\mathbf{r}) f(\mathbf{x} + \mathbf{r}). \quad (6)$$

Since we are interested in analyzing a compressible simulation, for the velocity field we use the Favre average $\tilde{u}(\mathbf{x}) = \bar{\rho}\bar{u}(\mathbf{x})/\bar{\rho}(\mathbf{x})$, (A. Favre 1975; H. Aluie 2011). The CG of the field f at a scale ℓ results in two contributions: the large scale field \bar{f}_ℓ , and the sub scale field $f' = f - \bar{f}_\ell$, the latter being the subgrid-scale (SGS) unresolved part of the original field f . By applying the CG to the set of Hall-MHD equations in Alfvén units (H. Aluie 2011, 2017; D. Manzini et al. 2022), we obtain the following SGS energy transfer terms (see Appendix

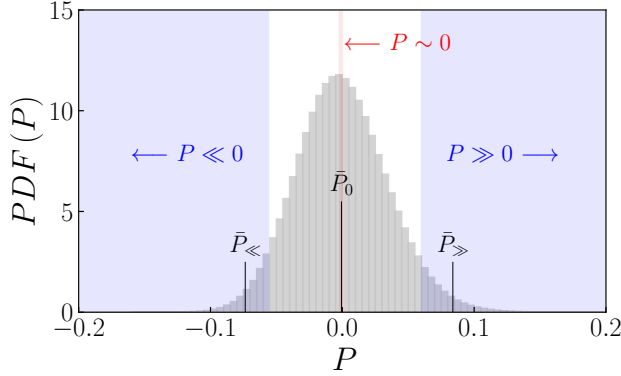


Figure 2. PDF of the first GTGI $P = -\nabla \cdot \mathbf{u}$. Shaded areas indicate $P \ll 0$, $P \gg 0$ (blue), and $P \sim 0$ (red) regimes. Vertical lines indicate the median values $\bar{P}_{\ll} = -0.06$, $\bar{P}_0 = -1.2 \times 10^{-3}$, and $\bar{P}_{\gg} = 0.07$ inside each subset.

A):

$$\pi_{sgs}^{\text{RM}} = -[\bar{\rho} \tilde{\tau}(u_j, u_k) - \bar{\tau}(b_j, b_k)] \partial_k \tilde{u}_j \quad (7)$$

$$\pi_{sgs}^{\text{BPY}} = -\frac{1}{\bar{\rho}} \partial_j \bar{p} \bar{\tau}(\rho, u_j) \quad (8)$$

$$\pi_{sgs}^{\text{MHD}} = -\mathcal{E}_j^{\text{MHD}} \bar{J}_j \quad (9)$$

$$\pi_{sgs}^{\text{Hall}} = -d_i \mathcal{E}_j^{\text{Hall}} \bar{J}_j, \quad (10)$$

where ρ is the density, $\bar{\tau}(f, g) = \overline{fg} - \bar{f}\bar{g}$ is the SGS stress tensor at scale ℓ , b_k is the magnetic field, p is the plasma pressure, J_k is the current density, d_i is the ion inertial length, $\mathcal{E}_k^{\text{MHD}} = \epsilon_{jkl}(\bar{u}_k \bar{b}_l - \bar{u}_l \bar{b}_k)$ and $\mathcal{E}_k^{\text{Hall}} = \epsilon_{jkl}(\bar{J}_k \bar{b}_l / \bar{\rho} - \bar{J}_l \bar{b}_k / \bar{\rho})$ are the MHD and Hall electromotive forces, respectively. The Reynolds-Maxwell (RM), MHD, and Hall energy transfer terms are the same of the incompressible case (e.g., see D. Manzini et al. 2022) with appropriate corrections due to density fluctuations (i.e., Favre filtering and $\bar{\rho}^{-1}$ factor in the Hall term). The baroclinal (BPY) work, instead, is a compressible-specific term due to the action of large-scale pressure gradients on turbulent mass fluxes (e.g., see H. Aluie 2011).

4. RESULTS

We analyze a three-dimensional box of a Hall-MHD simulation with $b_{rms} = u_{rms} = 0.25$, statistically vanishing $u \cdot b$ correlations, and resolution of $d_i/8$ at a fixed time. The numerical setup is described in Appendix B. To disentangle the different properties of compressible vs incompressible fluctuations we first present the statistics of the first velocity GTGI P , which is defined as $-\nabla \cdot \mathbf{u}$, see Equation (1). The probability distribution function (PDF) is reported in Figure 2. The obtained PDF is peaked around $P \sim 0$ and is slightly skewed towards positive values of the invariant ($skew = 0.23$). We divided

the PDF in three different regions: one representative of nearly-incompressible fluctuations, and two comprising the most compressible fluctuations in the negative and positive tails of the PDF. Such thresholds have been set as $P \ll 0$ below the 5% percentile of the PDF, $P \gg 0$ above the 95% percentile and $P \sim 0$ between 47.5% and 52.5% percentile, as indicated by the shaded areas in Figure 2, with the same sample size for the three cases.

To evaluate the energy transfer rate we need to set a scale ℓ for CG the fields. Hereafter we consider $\ell = d_i$ as a characteristic scale, where the turbulent cascade is transferring energy from scales greater than d_i , and Hall term effects as well as energy dissipation are contained at scales smaller than d_i . In this fashion we can evaluate the direct transfer of energy coming from the turbulent cascade towards sub-ion scales, and also the local energy coming from subgrid scales associated with sub-ion dynamics and Hall effect. Starting from the incompressible case, we report the joint PDF of Q and R evaluated after the CG of the velocity field at $\ell = d_i$ in Figure 3a. Although we filtered out the smallest-scale dissipative dynamics, the joint PDF still exhibits a notable asymmetry, with the tendency to develop a tail towards the $Q < 0$ and $R > 0$ part of the plane along the discriminant line $\Delta|_{P=\bar{P}_0}$, Equation (4). Since $\bar{P}_0 = -1.2 \times 10^{-3}$ is quite small, by calculating the separatrix between stable and unstable topologies $\bar{P}_0 Q - R = 0$ we obtain a curve very close to $R = 0$ that corresponds to the incompressible case (Figure 3). We then estimated the total energy transfer rate $\pi_{sgs} = \pi_{sgs}^{\text{RM}} + \pi_{sgs}^{\text{BPY}} + \pi_{sgs}^{\text{MHD}} + d_i \pi_{sgs}^{\text{Hall}}$ bin-averaged on the RQ -plane at $\ell = d_i$. Results are shown in Figure 3b. Only bins with more than 10 counts are considered in the joint PDF. We observe a strong self-organization of the turbulent energy flux with respect to the local streamline topology. A direct energy cascade organizes in a topological selective fashion on compressing strain (sheet-like) structures, and stable stretching vortical structures. Conversely, negative transfer rate has been found to be mostly associated with unstable compressing vortical structures. These results closely resemble recent findings in numerical simulations of hydrodynamic turbulence reported by H. Yao et al. (2024).

If we consider only compressible fluctuations, however, such a scenario changes. In Figure 4a-b we report the joint PDF of Q and R and the transfer rate π_{sgs} for the case $P \gg 0$. The joint PDF in this case is distorted if compared with the $P \sim 0$ case, following the discriminant line $\Delta|_{P=\bar{P}_{\gg}}$, where $\bar{P}_{\gg} = 0.07$ has been chosen to be the median value of the right tail in the $P \gg 0$ region, as shown in Figure 2. The energy transfer rate bin-averaged in the RQ -plane mostly develop positive

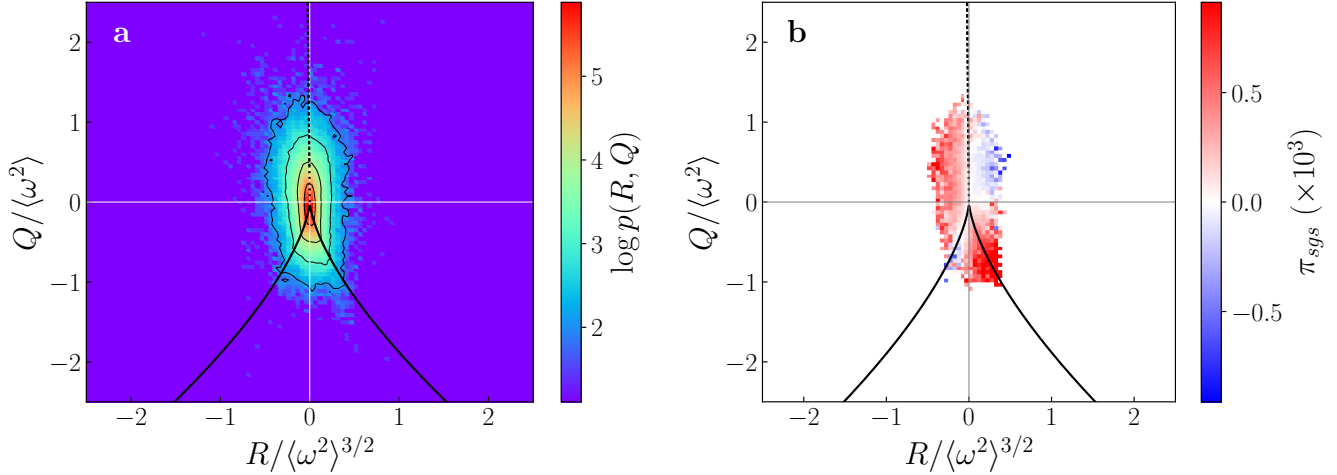


Figure 3. Joint PDFs of Q and R GTGIs (a) and averaged energy transfer rate in the RQ -plane (b) for $P \simeq 0$. GTGI values are normalized to powers of the enstrophy $\langle \omega^2 \rangle$. Thick black line indicate the discriminant for $\bar{P}_0 = -1.2 \times 10^{-3}$ and the dotted line indicate the $\bar{P}_0 Q - R = 0$ curve.

values with a net weakening of the topological selection observed in the incompressible case (i.e., a change of the topology in the RQ -plane does not correspond to a reversal of the energy transfer). The minimum values of π_{sgs} are organized along the $PQ - R = 0$ line separating unstable compressing vortical structures (1) from volume contracting topologies (5). Analogous, though opposite, results are obtained in the $P \ll 0$ case. In Figure 4c-d we show the joint PDF of Q and R and the transfer rate π_{sgs} , and the PDF is distorted in the opposite sense with respect to the $P \gg 0$ case. The shape of the PDF follows the discriminant line $\Delta|_{P=\bar{P}_{\ll}}$, Equation (4), where $\bar{P}_{\ll} = -0.06$ is the median value of the left tail in the $P \ll 0$ region showed in Figure 2. The opposite behavior is also observed in terms of total transfer rate, which tends to develop an inverse transfer almost everywhere on the plane, with a clear weakening along the $PQ - R = 0$ separatrix. We also observe nearly-vanishing values of π_{sgs} along the Vieillefosse tail, with even a few slightly positive bins. In compressible regions, the dominance of the cascade sign by P can be interpreted as a geometric effect: the local contraction (expansion) of the volume containing a certain amount of energy shifts this energy toward smaller (larger) scales. In other words, the volumetric compression itself acts as a cross-scale transfer mechanism.

5. DISCUSSIONS AND CONCLUSIONS

In this letter we elucidated the connection between local streamline topology and subgrid-scale energy transfer rate in both incompressible and compressible plasma regions. In nearly incompressible regions, the SGS energy transfer self-organizes with the streamline topology in the RQ -plane: strain-compressing and vortical-

stretching structures are associated with direct transfer rate towards small scales, whereas strain-stretching and vortical-compressing structures show a net back-transfer of energy from small scales. These results are shown for the particular choice of $\ell = d_i$, but similar properties can be also observed when moving towards inertial or sub-ion scales. As a matter of fact, the exact calculation of the transfer rate π_{sgs} in the space-filter approach is not based on Yaglom's law or other models, and can be properly applied at any CG scale (H. Aluie 2017; D. Manzini et al. 2022). Our results clearly highlight the primary role played by the velocity field in driving the LET rate, which nicely organizes in a topological selective fashion for nearly-incompressible fluctuations.

Concerning compressible subsets, the self-organization weakens and the sign of the transfer becomes primarily controlled by the local volumetric compression ($P > 0$) or expansion ($P < 0$), yielding predominantly forward transfer ($\pi_{sgs} > 0$) in compressing regions and predominantly inverse transfer ($\pi_{sgs} < 0$) on expanding sites. Although the sign of the first invariant P determines the net volumetric compression or expansion, it does not uniquely determine the local streamline topology, which depends upon individual eigenvalues. Hence, compressing and expanding subsets are still characterized by a co-existence of different topological configurations, such types (1) to (4) of Figure 1, although the direction of the energy transfer is primarily controlled by the sign of P . Previous studies have shown that at kinetic scales bulk and magnetic energy conversion are driven by the pressure-strain interaction (Y. Yang et al. 2016, 2017; D. Del Sarto & F. Pegoraro 2018; W. H. Matthaeus et al. 2020; O. Pezzi et al. 2021; Y. Yang et al. 2022; S.

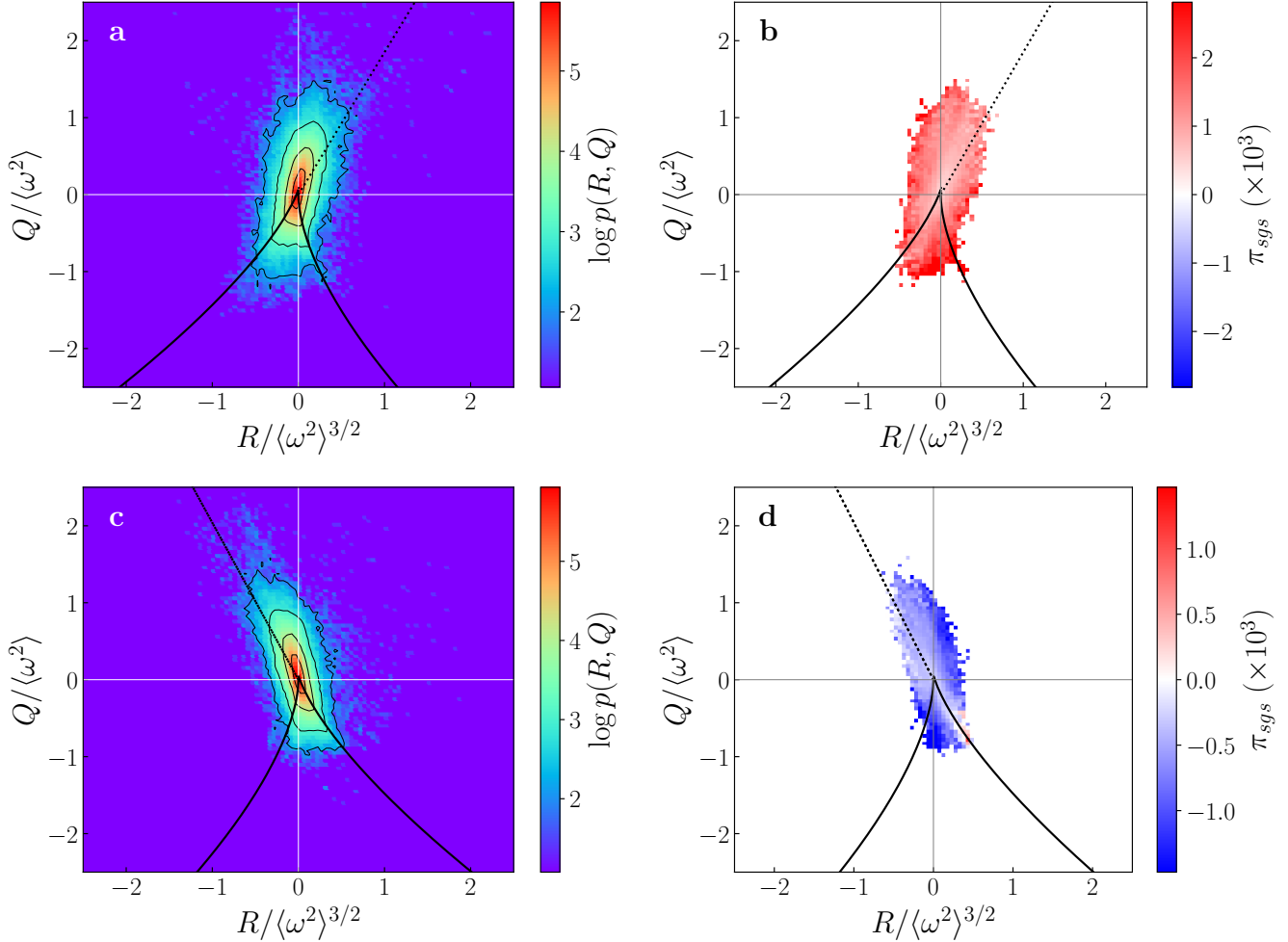


Figure 4. Joint PDFs of Q and R GTGIs (a) and averaged energy transfer rate in the RQ -plane (b) for $P \gg 0$. Thick black lines is the discriminant line obtained for $\bar{P}_{\parallel} = 0.07$ and the dotted line indicate the $\bar{P}_{\parallel} Q - R = 0$ curve. Joint PDFs of Q and R GTGIs (c) and averaged energy transfer rate in the RQ -plane (d) for $P \ll 0$. Thick black lines is the discriminant line obtained for $\bar{P}_{\parallel} = -0.06$ and the dotted line indicate the $\bar{P}_{\parallel} Q - R = 0$ curve. GTGI values are normalized to powers of the enstrophy $\langle \omega^2 \rangle$.

Roy et al. 2025; P. Hellinger & S. Landi 2025) in which the compressive part typically plays a subdominant role. Here we provide a complementary information by showing that where compressive fluctuations become significant at MHD/ion scales, they act as a cross-scale transfer mechanism for turbulent energy.

From a broader perspective, our findings indicate that the velocity GTGIs contain predictive information on the sign of the energy flux for nearly-incompressible fluctuations, that can be linked to the co-existence of direct and inverse energy transfer routinely observed in nearly-incompressible Alfvénic streams (C. W. Smith et al. 2009; J. T. Coburn et al. 2014). The strong correlation observed between streamline topology and energy transfer rate closely resembles previous observations in hydrodynamic turbulence in the incompressible case (F. van der Bos et al. 2002; H. Yao et al. 2024), extending

them to the case of Hall-MHD plasma turbulence in the more general and still unexplored compressible case. In compressible regions, indeed, we observe a weakening of the topological selection of the energy transfer, since the overall sign of π_{sgs} is determined by the sign of P (or equivalently $-\nabla \cdot \mathbf{u}$).

The study of the cascade rate associated with field line topology from an experimental point of view needs a multipoint constellation, and can be assessed in principle through missions like Cluster or MMS. Very recently, this kind of effort has been made by B. Hnat et al. (2025) on Cluster data, and authors conclude that magnetic field topology plays a role in the energy transfer rate by showing that a positive cascade rate is found to be associated with a predominance of strain-dominated magnetic field structures. This result supports the importance of reconnecting current sheets in driving the en-

ergy cascade towards small scales, also supported by several numerical studies (L. Franci et al. 2017; D. Manzini et al. 2023; R. Foldes et al. 2024). A dedicated investigation of the specific role of magnetic reconnection in the self-organization of magnetic field line structures from numerical simulations is here left as a future investigation.

All the dynamics of the energy cascade illustrated in this letter would greatly benefit from the simultaneous exploration of different spatial scales. The only way to test our results across different scales is to develop future multiscale constellation such as Helioswarm (K. G. Klein et al. 2023) and the proposed Plasma Observatory mission (J. Rae et al. 2022; A. Retinò et al. 2022), where different scales in heliospheric and magnetospheric plasmas can be simultaneously accessed in situ. In the context of a growing fleet of future multipoint and multiscale constellations, we emphasize the fundamental importance of including the study of the streamline topology by means of GTGI as a standard diagnostic for plasma turbulent studies. Indeed, whereas LET can give important insight about the local direction only of the energy cascade, the investigation of GTGIs adds the fundamental piece of information about the type of structures that

are locally transferring the energy, thus enabling a more comprehensive view of turbulent cascade in space plasmas.

ACKNOWLEDGMENTS

This work has been partially supported by Agenzia Spaziale Italiana (ASI) under the agreement ASI-INAF “Attività di Fase A per la missione Plasma Observatory” F83C24000690001. A.V. and G.C acknowledge partial financial support from the European Union – Next Generation EU – National Recovery and Resilience Plan (NRRP) – M4C2 Investment 1.1- PRIN 2022 (D.D. 104 del 2/2/2022) – Project “Modeling Interplanetary Coronal Mass Ejections”, MUR code 31. 2022M5TKR2, CUP B53D23004860006 and C53D23001190006. We acknowledge partial funding by “Fondazione Cassa di Risparmio di Firenze” under the project HIPER-CRHEL. E.P. acknowledges CINECA and INAF for awarding access to HPC resources under the coordination of the ”Accordo Quadro MoU per lo svolgimento di attività congiunta di ricerca Nuove frontiere in Astrofisica: HPC e Data Exploration di nuova generazione” (project INA23_C9A10).

REFERENCES

- Aluie, H. 2011, *PhRvL*, 106, 174502, doi: [10.1103/PhysRevLett.106.174502](https://doi.org/10.1103/PhysRevLett.106.174502)
- Aluie, H. 2017, *New Journal of Physics*, 19, 025008, doi: [10.1088/1367-2630/aa5d2f](https://doi.org/10.1088/1367-2630/aa5d2f)
- Aluie, H., & Eyink, G. L. 2010, *PhRvL*, 104, 081101, doi: [10.1103/PhysRevLett.104.081101](https://doi.org/10.1103/PhysRevLett.104.081101)
- Biferale, L., Chevillard, L., Meneveau, C., & Toschi, F. 2007, *PhRvL*, 98, 214501, doi: [10.1103/PhysRevLett.98.214501](https://doi.org/10.1103/PhysRevLett.98.214501)
- Bruno, R., & Carbone, V. 2016, *Turbulence in the Solar Wind*, Vol. 928, doi: [10.1007/978-3-319-43440-7](https://doi.org/10.1007/978-3-319-43440-7)
- Burch, J. L., Moore, T. E., Torbert, R. B., & Giles, B. L. 2016, *SSRv*, 199, 5, doi: [10.1007/s11214-015-0164-9](https://doi.org/10.1007/s11214-015-0164-9)
- Camporeale, E., Sorriso-Valvo, L., Califano, F., & Retinò, A. 2018, *Phys. Rev. Lett.*, 120, 125101, doi: [10.1103/PhysRevLett.120.125101](https://doi.org/10.1103/PhysRevLett.120.125101)
- Chertkov, M., Pumir, A., & Shraiman, B. I. 1999, *Physics of Fluids*, 11, 2394, doi: [10.1063/1.870101](https://doi.org/10.1063/1.870101)
- Coburn, J. T., Smith, C. W., Vasquez, B. J., Forman, M. A., & Stawarz, J. E. 2014, *ApJ*, 786, 52, doi: [10.1088/0004-637X/786/1/52](https://doi.org/10.1088/0004-637X/786/1/52)
- Consolini, G., Materassi, M., Federica Marcucci, M., & Pallocchia, G. 2015, *ApJ*, 812, 84, doi: [10.1088/0004-637X/812/1/84](https://doi.org/10.1088/0004-637X/812/1/84)
- Dallas, V., & Alexakis, A. 2013, *Physics of Fluids*, 25, 105106, doi: [10.1063/1.4824195](https://doi.org/10.1063/1.4824195)
- Del Sarto, D., & Pegoraro, F. 2018, *MNRAS*, 475, 181, doi: [10.1093/mnras/stx3083](https://doi.org/10.1093/mnras/stx3083)
- Escoubet, C. P., Schmidt, R., & Goldstein, M. L. 1997, *SSRv*, 79, 11, doi: [10.1023/A:1004923124586](https://doi.org/10.1023/A:1004923124586)
- Eyink, G. L. 2005, *Physica D Nonlinear Phenomena*, 207, 91, doi: [10.1016/j.physd.2005.05.018](https://doi.org/10.1016/j.physd.2005.05.018)
- Favre, A. 1975, in In: CANCAM 75; *Proceedings of the Fifth Canadian Congress of Applied Mechanics*, G3–G34
- Foldes, R., Cerri, S. S., Marino, R., & Camporeale, E. 2024, *PhRvE*, 110, 055207, doi: [10.1103/PhysRevE.110.055207](https://doi.org/10.1103/PhysRevE.110.055207)
- Franci, L., Landi, S., Verdini, A., Matteini, L., & Hellinger, P. 2018, *ApJ*, 853, 26, doi: [10.3847/1538-4357/aaa3e8](https://doi.org/10.3847/1538-4357/aaa3e8)
- Franci, L., Cerri, S. S., Califano, F., et al. 2017, *ApJL*, 850, L16, doi: [10.3847/2041-8213/aa93fb](https://doi.org/10.3847/2041-8213/aa93fb)
- Germano, M. 1992, *Journal of Fluid Mechanics*, 238, 325, doi: [10.1017/S0022112092001733](https://doi.org/10.1017/S0022112092001733)
- Hellinger, P., & Landi, S. 2025, *A&A*, 704, A131, doi: [10.1051/0004-6361/202556752](https://doi.org/10.1051/0004-6361/202556752)

- Hnat, B., Chapman, S. C., Liptrott, C. M., & Watkins, N. W. 2025, *Physical Review Research*, 7, 043058, doi: [10.1103/9wb2-r437](https://doi.org/10.1103/9wb2-r437)
- Hnat, B., Chapman, S. C., & Watkins, N. W. 2021, *PhRvL*, 126, 125101, doi: [10.1103/PhysRevLett.126.125101](https://doi.org/10.1103/PhysRevLett.126.125101)
- Klein, K. G., Spence, H., Alexandrova, O., et al. 2023, *SSRv*, 219, 74, doi: [10.1007/s11214-023-01019-0](https://doi.org/10.1007/s11214-023-01019-0)
- Manzini, D., Sahraoui, F., & Califano, F. 2023, *PhRvL*, 130, 205201, doi: [10.1103/PhysRevLett.130.205201](https://doi.org/10.1103/PhysRevLett.130.205201)
- Manzini, D., Sahraoui, F., Califano, F., & Ferrand, R. 2022, *PhRvE*, 106, 035202, doi: [10.1103/PhysRevE.106.035202](https://doi.org/10.1103/PhysRevE.106.035202)
- Marino, R., & Sorriso-Valvo, L. 2023, *PhR*, 1006, 1, doi: [10.1016/j.physrep.2022.12.001](https://doi.org/10.1016/j.physrep.2022.12.001)
- Matthaeus, W. H., Yang, Y., Wan, M., et al. 2020, *ApJ*, 891, 101, doi: [10.3847/1538-4357/ab6d6a](https://doi.org/10.3847/1538-4357/ab6d6a)
- Meneveau, C. 2011, *Annual Review of Fluid Mechanics*, 43, 219, doi: [10.1146/annurev-fluid-122109-160708](https://doi.org/10.1146/annurev-fluid-122109-160708)
- Montagud-Camps, V., Němcová, F., Šafránková, J., et al. 2021, *Atmosphere*, 12, 1162, doi: [10.3390/atmos12091162](https://doi.org/10.3390/atmos12091162)
- Pezzi, O., Liang, H., Juno, J. L., et al. 2021, *MNRAS*, 505, 4857, doi: [10.1093/mnras/stab1516](https://doi.org/10.1093/mnras/stab1516)
- Politano, H., & Pouquet, A. 1998, *PhRvE*, 57, R21, doi: [10.1103/PhysRevE.57.R21](https://doi.org/10.1103/PhysRevE.57.R21)
- Quattrociocchi, V., Consolini, G., Marcucci, M. F., & Materassi, M. 2019, *ApJ*, 878, 124, doi: [10.3847/1538-4357/ab1e47](https://doi.org/10.3847/1538-4357/ab1e47)
- Quattrociocchi, V., Consolini, G., Materassi, M., Verdini, A., & Papini, E. 2025, *Chaos Solitons and Fractals*, 191, 115900, doi: [10.1016/j.chaos.2024.115900](https://doi.org/10.1016/j.chaos.2024.115900)
- Rae, J., Forsyth, C., Dunlop, M., et al. 2022, *Experimental Astronomy*, 54, 391, doi: [10.1007/s10686-022-09861-w](https://doi.org/10.1007/s10686-022-09861-w)
- Retinò, A., Khotyaintsev, Y., Le Contel, O., et al. 2022, *Experimental Astronomy*, 54, 427, doi: [10.1007/s10686-021-09797-7](https://doi.org/10.1007/s10686-021-09797-7)
- Roy, S., Bandyopadhyay, R., Adhikari, S., Yang, Y., & Matthaeus, W. H. 2025, *Physics of Plasmas*, 32, 112302, doi: [10.1063/5.0278907](https://doi.org/10.1063/5.0278907)
- Smith, C. W., Stawarz, J. E., Vasquez, B. J., Forman, M. A., & MacBride, B. T. 2009, *PhRvL*, 103, 201101, doi: [10.1103/PhysRevLett.103.201101](https://doi.org/10.1103/PhysRevLett.103.201101)
- Sorriso-Valvo, L., Perrone, D., Pezzi, O., et al. 2018, *Journal of Plasma Physics*, 84, 725840201, doi: [10.1017/S0022377818000302](https://doi.org/10.1017/S0022377818000302)
- Sorriso-Valvo, L., Catapano, F., Retinò, A., et al. 2019, *PhRvL*, 122, 035102, doi: [10.1103/PhysRevLett.122.035102](https://doi.org/10.1103/PhysRevLett.122.035102)
- Stawarz, J. E., Smith, C. W., Vasquez, B. J., Forman, M. A., & MacBride, B. T. 2010, *ApJ*, 713, 920, doi: [10.1088/0004-637X/713/2/920](https://doi.org/10.1088/0004-637X/713/2/920)
- Suman, S., & Girimaji, S. S. 2010, *Journal of Turbulence*, 11, 2, doi: [10.1080/14685241003604751](https://doi.org/10.1080/14685241003604751)
- Vaghefi, N. S., & Madnia, C. K. 2015, *Journal of Fluid Mechanics*, 774, 67, doi: [10.1017/jfm.2015.235](https://doi.org/10.1017/jfm.2015.235)
- van der Bos, F., Tao, B., Meneveau, C., & Katz, J. 2002, *Physics of Fluids*, 14, 2456, doi: [10.1063/1.1472506](https://doi.org/10.1063/1.1472506)
- Vela-Martín, A., & Jiménez, J. 2021, *Journal of Fluid Mechanics*, 915, A36, doi: [10.1017/jfm.2021.105](https://doi.org/10.1017/jfm.2021.105)
- Vieillefosse, P. 1982, *Journal de Physique*, 43, 837, doi: [10.1051/jphys:01982004306083700](https://doi.org/10.1051/jphys:01982004306083700)
- Vieillefosse, P. 1984, *Physica A Statistical Mechanics and its Applications*, 125, 150, doi: [10.1016/0378-4371\(84\)90008-6](https://doi.org/10.1016/0378-4371(84)90008-6)
- Wang, L., & Lu, X.-Y. 2012, *Journal of Fluid Mechanics*, 703, 255, doi: [10.1017/jfm.2012.212](https://doi.org/10.1017/jfm.2012.212)
- Yang, Y., Matthaeus, W. H., Roy, S., et al. 2022, *ApJ*, 929, 142, doi: [10.3847/1538-4357/ac5d3e](https://doi.org/10.3847/1538-4357/ac5d3e)
- Yang, Y., Matthaeus, W. H., Shi, Y., Wan, M., & Chen, S. 2017, *Physics of Fluids*, 29, 035105, doi: [10.1063/1.4979068](https://doi.org/10.1063/1.4979068)
- Yang, Y., Shi, Y., Wan, M., Matthaeus, W. H., & Chen, S. 2016, *PhRvE*, 93, 061102, doi: [10.1103/PhysRevE.93.061102](https://doi.org/10.1103/PhysRevE.93.061102)
- Yao, H., Schnaubelt, M., Szalay, A. S., Zaki, T. A., & Meneveau, C. 2024, *Journal of Fluid Mechanics*, 980, A42, doi: [10.1017/jfm.2023.1066](https://doi.org/10.1017/jfm.2023.1066)
- Zhang, J., Huang, S. Y., Sahraoui, F., et al. 2023, *Journal of Geophysical Research (Space Physics)*, 128, e2022JA031064, doi: [10.1029/2022JA031064](https://doi.org/10.1029/2022JA031064)
- Zheng, Q., Yang, Y., Wang, J., & Chen, S. 2022, *Journal of Fluid Mechanics*, 950, A21, doi: [10.1017/jfm.2022.742](https://doi.org/10.1017/jfm.2022.742)

APPENDIX

A. COARSE-GRAINED COMPRESSIBLE HALL-MHD EQUATIONS

In this work we use the SGS energy transfer terms arising from the CG of the compressible Hall-MHD equations. In this section we summarize the derivation of all the energy transfer terms denoted as π_{sgs} . The set of compressible Hall-MHD equations comprises the continuity equation

$$\partial_t \rho + \partial_j (\rho u_j) = 0, \quad (\text{A1})$$

the momentum equation

$$\partial_t (\rho u_j) + \partial_k \left[\rho u_j u_k + \left(p + \frac{b^2}{2} \right) \delta_{jk} - b_j b_k \right] = \mathcal{D}_j^{(u)}, \quad (\text{A2})$$

and the induction equation

$$\partial_t b_j = \epsilon_{jkl} \partial_k \left[\epsilon_{lmn} u_m b_n - d_i \epsilon_{lmn} \frac{J_m b_n}{\rho} \right] + \mathcal{D}_j^{(b)}. \quad (\text{A3})$$

In these equations d_i is the ion inertial length, and $\mathcal{D}_j^{(u)}$, $\mathcal{D}_j^{(b)}$ indicate the dissipative terms that are not explicitly written since they do not contribute to the SGS energy transfer. By filtering the equations with a Gaussian kernel, we indicate with \bar{f} the filtered version of the field f and with $\tilde{u}_i = \overline{\rho u_i}/\bar{\rho}$ the Favre filtered version of the velocity field. We then define the stress tensor $\bar{\tau}(f, g) = \overline{f g} - \bar{f} \bar{g}$ along with its Favre filtered version for the velocity field $\tilde{\tau}(u_i, u_j) = \overline{u_i u_j} - \tilde{u}_i \tilde{u}_j$. The coarse-grained versions of the compressible Hall-MHD equations are

$$\partial_t \bar{\rho} + \partial_j (\bar{\rho} \tilde{u}_j) = 0 \quad (\text{A4})$$

for the continuity equation, then

$$\partial_t (\bar{\rho} \tilde{u}_j) + \partial_k \left[\bar{\rho} \tilde{u}_j \tilde{u}_k + \left(\bar{p} + \frac{\bar{b}^2}{2} \right) \delta_{jk} - \bar{b}_j \bar{b}_k \right] = -\partial_k [\bar{\rho} \tilde{\tau}(u_j, u_k) - \bar{\tau}(b_j, b_k)] + \bar{\mathcal{D}}_j^{(u)} \quad (\text{A5})$$

for the momentum equation, and

$$\partial_t \bar{b}_j = \epsilon_{jkl} \partial_k \left[\epsilon_{lmn} \left(\tilde{u}_m \bar{b}_n - d_i \frac{\bar{J}_m \bar{b}_n}{\bar{\rho}} \right) + \mathcal{E}_l^{\text{MHD}} - d_i \mathcal{E}_l^{\text{Hall}} \right] + \bar{\mathcal{D}}_j^{(b)} \quad (\text{A6})$$

for the induction equation. The terms $\mathcal{E}_l^{\text{MHD}} = \overline{\epsilon_{lmn} u_m b_n} - \epsilon_{lmn} \tilde{u}_m \bar{b}_n$ and $\mathcal{E}_l^{\text{Hall}} = \overline{\epsilon_{lmn} J_m b_n / \rho} - \epsilon_{lmn} \bar{J}_m \bar{b}_n / \bar{\rho}$ indicate the MHD and Hall electromotive forces, respectively. By multiplying Equation (A5) for \tilde{u}_j and Equation (A6) for \bar{b}_j , we can calculate the rate of change of kinetic and magnetic energy, and by introducing the term \mathcal{F}_k containing all the contributions that can be written as spatial fluxes (i.e., written in divergence form), we obtain the total energy balance as

$$\partial_t (\bar{E}_u + \bar{E}_b) + \partial_k \mathcal{F}_k = -\bar{p} \partial_j \tilde{u}_j - \pi_{sgs} + \tilde{u}_j \bar{\mathcal{D}}_j^{(u)} + \bar{b}_j \bar{\mathcal{D}}_j^{(b)}, \quad (\text{A7})$$

where the spatial flux term is

$$\begin{aligned} \mathcal{F}_k = \bar{E}_u \tilde{u}_k + \bar{p} \tilde{u}_j \delta_{jk} + \frac{\bar{b}^2}{2} \tilde{u}_j - \tilde{u}_j \bar{b}_j \bar{b}_k - d_i \epsilon_{jkl} \frac{\epsilon_{lmn} \bar{J}_m \bar{b}_n}{\bar{\rho}} \bar{b}_l \\ + \bar{\rho} \tilde{u}_j \tilde{\tau}(u_j, u_k) - \tilde{u}_j \bar{\tau}(b_j, b_k) - \bar{J}_k (\mathcal{E}_k^{\text{MHD}} + d_i \mathcal{E}_k^{\text{Hall}}) \end{aligned} \quad (\text{A8})$$

and the subgrid energy transfer term is

$$\begin{aligned} \pi_{sgs} = -[\bar{\rho} \tilde{\tau}(u_j, u_k) - \bar{\tau}(b_j, b_k)] \partial_k \tilde{u}_j - \frac{1}{\bar{\rho}} \partial_j \bar{p} \bar{\tau}(\rho, u_j) - \mathcal{E}_j^{\text{MHD}} \bar{J}_j - d_i \mathcal{E}_j^{\text{Hall}} \bar{J}_j \\ = \pi_{sgs}^{\text{RM}} + \pi_{sgs}^{\text{BPY}} + \pi_{sgs}^{\text{MHD}} + d_i \pi_{sgs}^{\text{Hall}}. \end{aligned} \quad (\text{A9})$$

Superscript indices refer to Reynolds-Maxell (RM) stress tensor, baropycnal (BPY) work, MHD, and Hall SGS energy transfer rate.

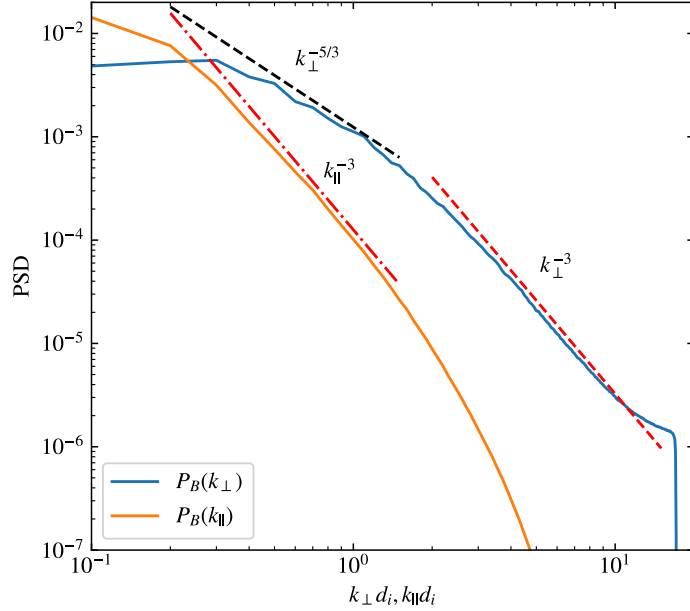


Figure 5. Reduced 1D perpendicular and parallel spectra of magnetic field fluctuations w.r.t the mean magnetic field. Dashed and dot-dashed lines represent typical slopes expected in inertial and Hall ranges that serve as reference.

B. NUMERICAL SETUP

In this work, we employ a pseudospectral code that solves the compressible viscous-resistive Hall-MHD equations (V. Montagud-Camps et al. 2021). In the code, all physical quantities are normalized with respect to a characteristic length $L = d_i$ set to be equal to the ion inertial length, a plasma density ρ_0 , a magnetic field amplitude B_0 , and a pressure $P_0 = \rho_0 c_A^2$ (being $c_A = B_0 / \sqrt{4\pi\rho_0}$ the Alfvén speed). Dynamic viscosity μ and magnetic resistivity η are in units of $d_i c_A \rho_0$ and $d_i c_A$ respectively. The simulation box consists of a cube with periodic boundaries whose edge is $20\pi d_i$ long. A grid of 512^3 points is employed, corresponding to a spatial resolution of $0.1227 d_i$ in all three directions. There is a mean background magnetic field along \hat{x} , i.e., $\mathbf{B}_0 = B_0 \hat{x}$. The simulation is initialized with a spectrum of fluctuations with constant amplitudes, random phases, and zero-mean cross-helicity (L. Franci et al. 2018). The amplitudes of magnetic and velocity fluctuations are set such that the root mean square of the fluctuations is $B_{rms} = u_{rms} = 0.25$. Finally, we set the plasma $\beta = 2P_0/B_0^2 = 2$, $\nu = \eta = 10^{-3}$, corresponding to a Reynolds number of 4000. The simulation evolves as a classic Alfvénic decaying turbulence simulation. The dataset employed in this work corresponds to a snapshot of the simulation taken at the time when turbulence has fully developed. The reduced 1D power spectra of magnetic field fluctuations are displayed in Figure 5, and give similar spectral properties to those reported by L. Franci et al. (2018) for 3D hybrid numerical simulations of turbulence. In particular, the parallel 1D reduced spectrum exhibit a slope $\sim k_{\parallel}^{-3}$, while the reduced 1D perpendicular spectrum shows an inertial range, $\sim k_{\perp}^{-5/3}$ below $k_{\perp} d_i = 1$, and then develops a $\sim k_{\perp}^{-3}$ trend at sub-ion scales.